


# State of Charge Estimation of Using Luenberger, Sliding Mode and Super twisting Observers

Qudus Ayinde AROMOSE <sup>1,†,‡</sup> , Stefan George ROSU <sup>2,‡</sup>

<sup>1</sup> Affiliation 1; qudus.aromose@stud.etti.upb.ro

<sup>2</sup> Affiliation 2; stefan.rosu@upb.ro

\* Correspondence: qudus.aromose@stud.etti.upb.ro;

<sup>†</sup> Current address: National University of Science and Technology POLITEHNICA Bucharest.

<sup>‡</sup> These authors contributed equally to this work.

**Abstract:** Lithium-ion batteries have been widely applied in many energy storage systems, such as electrical vehicles (EVs). The Battery Management System (BMS) is a crucial technology for EVs that use batteries to store energy, and it ensures the safety and well-functioning operation of the car. The state of charge (SOC) is one of the significant parameters to be measured to assure the optimal use of the amount of energy present in a battery, and its accuracy has a direct impact on the BMS behaviour. This paper compares three estimations: Luenberger Observer, Sliding Mode Observer (SMO), and Super Twisting Observer (STO). SMO and STO constitute a robust control technique against modelling errors and uncertainties present in inaccurate battery models. Finally, according to the SOC estimation tests, the SMO method presents the fastest convergence speed in comparison with the Luenberger Observer and Super Twisting Observer (STO), and its undesired chattering is reduced by the STO method.

**Keywords:** Li-Pb Battery; Sliding Mode Observer (SMO); SOC Estimation; Electric Vehicles (EVs); State of Charge

## 1. Introduction

The deployment of EVs in the world's transport fleet is part of the attempt to reduce greenhouse gas emissions as part of the Paris Agreement adopted by 196 Parties at COP21 in Paris, a legally binding international treaty on climate change [1]. The goal is to limit global temperature rise to a maximum of 2 degrees Celsius, preferably to 1.5 degrees Celsius compared to pre-industrial levels. In 2021, at the COP26 in Glasgow, the declaration on accelerating the transition to 100 % zero-emission cars and vans was signed by 27 governments in developed countries, 10 governments in emerging markets and developing economies, and 46 cities, states and regional governments alongside automotive manufacturers, fleet owners, operators, investors, and financial institutions [2]. The agreement sets commitments for the future of the electric vehicles market, and together, they aim for all sales of new cars and vans to be zero emission globally by 2040 and no longer than 2035 in leading markets.

This urge for the development of better EVs is not only climate-related; in addition, they have better efficiency in comparison with conventional internal combustion engine (ICE) vehicles, and with the emergence of new technologies, the price tends to decrease. Lithium-ion batteries (LIBs) are used as the primary source of energy storage systems. However, their high cost and highly dynamic nature limit their application in EVs[3].

Received:

Revised:

Accepted:

Published:

**Citation:** . State of Charge Estimation of Li-Pb battery Using Luenberger, Sliding Mode and Super twisting Observers. *Journal Not Specified* **2025**, *1*, 0. <https://doi.org/>

**Copyright:** © 2025 by the authors.

Submitted to *Journal Not Specified* for possible open access publication under the terms and conditions of the Creative Commons Attribution (CC BY) license (<https://creativecommons.org/licenses/by/4.0/>).

Given the highly nonlinear nature of the LIBs batteries, an efficient Battery Management System (BMS) is required to operate in the safe region by monitoring the battery constraints. Parameters such as the State of Charge (SOC), State of Health (SOH), State of Energy (SOE), State of Power (SOP), and State of Function (SOF) are used by the BMS to ensure the well-functioning systems[3], [4], [5]. The SOC estimation is a significant parameter for the optimal charge and discharge operation of LIB batteries in electronic devices and EVs, and the improvement of its accuracy has been developed in different papers in the literature. Reports show that document development in state-of-charge methods has been growing significantly in the last decade[3]

Figure 1 presents the overall process of model-based SOC estimation, which can be divided into two steps: battery modelling and algorithm implementation. Analysing the different modellings in the literature, the electrical equivalent circuit model (EECM) can obtain the best trade-off between model complexity and accuracy.

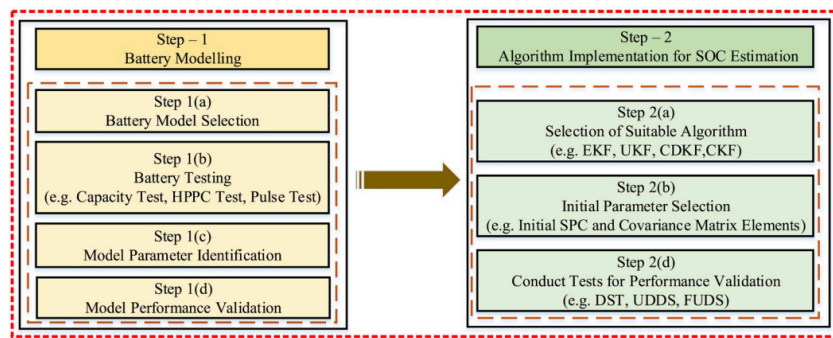


**Figure 1.** Overall process of the model-based SOC estimation [3].

There are several SOC estimation methods in the literature, and analysing the advantages and gaps between them can help BMS engineers select the right technology for specific scenarios and applications. The Non-Linear Observers (NLO) are part of the solution for the SOC estimation problem, and within the NLO scope, we can cite: Sliding Mode Observer (SMO); Proportional Integral Observer (PIO); Non-linear Observer (NLO) [6]

The SMO constitutes an advantageous method for model-based SOC because of its properties, such as robust control against modelling errors and uncertainties. Kim et al. [7] have shown that SMO properties play a major role in compensating for errors when the cell model is not accurate enough, converging to the expected result within a finite time. Hence, this paper aims to address the SOC estimation problem using the SMO alongside a deep comparison with other observers present in literature, such as the Luenberger observer (or State Observer), and Super Twisting Observer (STO).

The paper is organized as follows. Section 2 introduces the concept of state-of-charge estimation and how the problem is addressed. Section 3 presents the battery modelling used in the simulation described by Kim et al. [7]. Section 4 addresses the observers used to perform the SOC estimation. Section 5 presents the observer's estimations and comparisons of the final results obtained with two different tests: Constant current discharge and Urban Dynamometer Driving Schedule (UDDS) cycle discharge.

## 2. Concept of State of Charge Estimation

One of the most essential features of a BMS is the accurate estimation of the SOC. The BMS controls the charging of the battery according to its properties and charge state. It controls the battery discharging based on the load demand and the charge available in the battery systems. The battery cell voltage levels need to be measured by the BMS to estimate the charge states of the battery cells and to protect the cells from overcharging and undercharging [8].

The SOC is defined as the ratio between the remaining energy capacity ( $E_{cr}$ ) and the actual energy capacity ( $E_{ca}$ ) of the battery, as presented in Equation (1) [3]. The remaining energy is the maximum available capacity in the battery after a specific period of time, and the degradation of electrochemical properties caused by cycling and corrosion has an influence on its value. In contrast with  $E_{cr}$ , the actual energy is the maximum possible limit of charge in the battery obtained during the initial charge and discharge cycle considering different environmental conditions.

Battery SOC performs a similar operation to the fuel gauge in a gasoline-driven vehicle, indicating how much energy is left inside a battery to power a vehicle [6]. Figure 2 presents the SOC expressed in percentage, where 100% is the fully charged battery and 0% fully discharged.

$$\text{SOC}(t) = \frac{E_{cr}}{E_{ca}} \times 100. \quad (1)$$

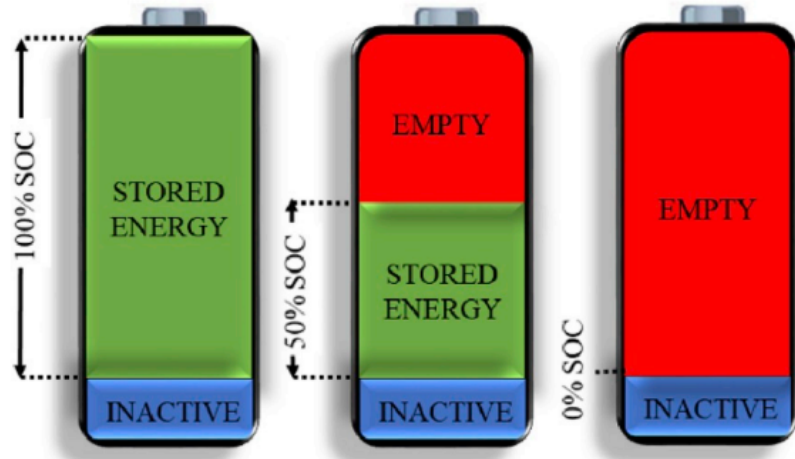


**Figure 2.** Stored energy for 100 %, 50 %, and 0 % SOC's [3].

Since no sensor can measure SOC, it should be estimated from physical measurements by some mathematical algorithm. The SOC error is confined to the acceptable level, less than 3 % in most cases which is applicable to the actual environments [7]

### 3. Battery Modelling

To maintain the trade-off between battery model complexity and accuracy, the modelling approach EECM has been used in many SOC methods present in the literature [7], [8], [9]. Furthermore, the EECM is the most promising modelling for online battery parameters and state estimation in the field of EV applications, and it uses components such as resistors, capacitors, and voltage sources to simulate the dynamic behaviour of the battery. This approach is organized into three categories: Rint mode, Randles model, and RC mode [6]. Figure 3 presents the RC model used in this paper.

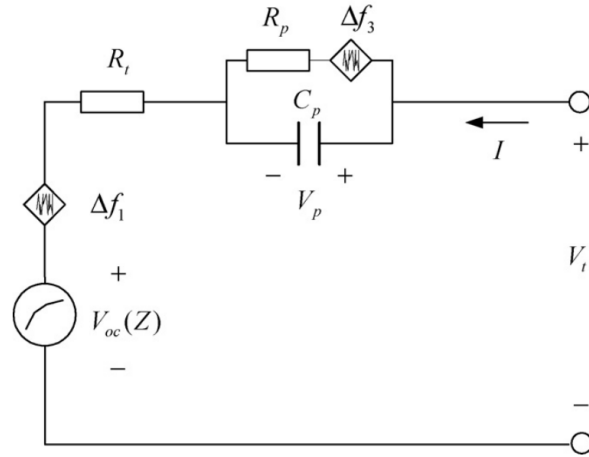


**Figure 3.** Resistor-capacitor electrical model of lithium-ion battery [7].

The RC model has a non-linear voltage source  $V_{oc}(Z)$  as a function of the SOC ( $Z$ ), ohmic resistance ( $R_t$ ), parallel-connected polarization capacitance ( $C_p$ ), and polarization resistance ( $R_p$ ). Thus,  $V_{oc}$  varies in the range of SOC, and  $Z$  varies from 0% to 100%. According to Figure 3,  $V_t$  can be written as follows:

$$V_t = V_{oc}(Z) + IR_t + V_p. \quad (2)$$

The time derivatives of polarization voltage and the SOC are described below:

$$\dot{Z} = \frac{I}{C_n} = \frac{1}{R_t C_n} (V_t - V_{oc}(Z) - V_p), \quad \dot{V}_p = -\frac{V_p}{R_p C_p} + \frac{I}{C_p}, \quad (3)$$

where  $C_n$  is the nominal capacity of the cell.

The non-linearity relationship of OCV–SOC is shown in Figure 4. Regardless of the non-linear behavior, there is a piecewise linear relationship between the two parameters as shown in the range indicated by the dots in the curve. Therefore, the linear model  $V_{oc}(Z) = kZ + d$  is defined for a range of the SOC. Hence,  $k$  and  $d$  are constant for a certain range of  $Z$ . Furthermore, the time derivative of  $V_{oc}$  is obtained as:

$$\dot{V}_{oc}(Z) = k\dot{Z} = k\left(\frac{I}{C_n}\right). \quad (4)$$

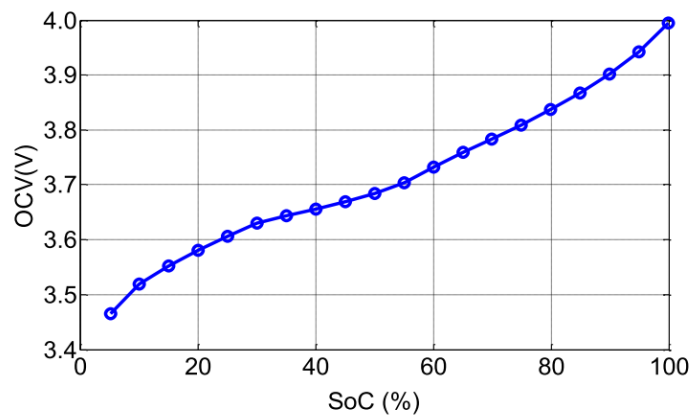


**Figure 4.** OCV-SOC curve for a lithium-ion polymer cell [10].

The current is assumed to be constant, which means that  $dI/dt = 0$ , and the time derivative of  $\dot{V}_t$  is presented below:

$$\dot{V}_{oc}(Z) = k\left(\frac{I}{C_n}\right) + \frac{V_p}{R_p C_p} - \frac{I}{C_p}. \quad (5)$$

Rearranging the equations and substituting  $V_p = V_t - V_{oc} - IR_t$  in Eq. (5), results in the state-space equations of the EECM model:

$$\begin{aligned} \dot{V}_t &= -a_1 V_t + a_1 V_{oc}(Z) + b_1 I, \\ \dot{Z} &= a_2 V_t - a_2 V_{oc}(Z) - a_2 V_p, \\ \dot{V}_p &= -a_1 V_p + b_2 I, \\ y &= \begin{bmatrix} 1 & 0 & 0 \end{bmatrix} \begin{bmatrix} V_t \\ Z \\ V_p \end{bmatrix}, \end{aligned} \quad (6)$$

where  $a_1 = 1/(R_t C_p)$ ,  $a_2 = 1/(R_t C_n)$ ,  $b_1 = k/C_n + R_t/(R_p C_p) + 1/C_p$ , and  $b_2 = 1/C_p$ .

This model is not accurate in comparison with the real cell as the piecewise linearization given by  $V_{oc} = kZ + d$  is used to describe the relationship of OCV-SOC, and its parameters  $k$  and  $d$  are taken as constants instead of varying according to the SOC. Therefore, the nonlinearities caused by the linearization error  $d$  and all modeling errors, uncertainties, and time varying related to the RC model are considered external disturbances described as  $\Delta f_i$ :

$$\begin{aligned} \dot{V}_t &= -a_1 V_t + a_1 kZ + b_1 I + \Delta f_1 = -a_1 V_t + a_{11}Z + b_1 I + \Delta f_1, \\ \dot{Z} &= a_2 V_t - a_2 kZ - a_2 V_p + \Delta f_2 = a_{12}V_t - a_{22}Z - a_2 V_p + \Delta f_2, \\ \dot{V}_p &= -a_1 V_p + b_2 I + \Delta f_3, \end{aligned} \quad (7)$$

where  $\Delta f_1 = \Gamma_1 \xi$ ,  $\Delta f_2 = \Gamma_2 \xi$ , and  $\Delta f_3 = \Gamma_3 \xi$ . The parameters  $\Gamma_i$  are known values and  $\xi$  represents an unknown bounded value.

Furthermore, the computation of the observability matrix ( $O_M$ ) of the state-space system is used to assure that the cell model is observable. From the classical approach of control system theory, the system is observable if and only if  $\text{rank}(O_M) = n$ , where  $n$  is the dimension of state-space variable  $\dim(x) = n$  [11]. Equation (8) is shown as follow:

$$O_M = \begin{bmatrix} C \\ CA \\ CA^2 \end{bmatrix}, \quad (8)$$

where  $C = \begin{bmatrix} 1 & 0 & 0 \end{bmatrix}$ , and  $A$  is the system parameter matrix presented in Equation (7). The observability matrix is computed as shown above.

$$O_M = \begin{bmatrix} 1 & 0 & 0 \\ -a_1 & a_{11} & 0 \\ a_1^2 + a_2 a_{11} & -a_1 a_{11} - a_1 a_{22} & -a_2 a_{11} \end{bmatrix} \quad (9)$$

Hence, the proposed battery modeling is observable for every operating condition as the observability matrix is always full rank.

### 3.1 Battery Modeling Parameter Extraction

Kim *et al.* [7] has used a large-size Li-Pb battery cell for testing, aiming at the extraction of the cell parameters. The cell has a nominal capacity of 5.0 Ah, and a nominal voltage of 3.8 V with dimensions of 250 mm × 125 mm × 5 mm and a weight of 120 g. A thermal chamber was used to regulate the temperature to 25°C, and the charge-discharge equipment Nittetsu cyler was used to simulate the cell's discharge. During the test, the true SOC is directly obtained using the ampere-hour method.

The test is comprised of a sequence of constant current discharges for 180 s and rests for 3600 s until the battery is fully discharged. Initially, the cell started fully charged up to 4.2 V, and the discharge current is 5 A. This amount represents 1  $C_n$  rate considering the nominal capacity, and the SOC will decrease 5% for each period.

Finally, the parameters for the state modeling were adjusted to the real cell data. Hence, the model parameters are given as  $a_1 = 1.667$ ,  $a_2 = 0.0589$ ,  $a_{11} = 2.8339$ ,  $a_{22} = 0.1001$ ,  $b_1 = 0.00672$ ,  $b_2 = 0.005$  [7]. Further, the uncertainties are computed by this same comparison with the true cell results in order to minimize the errors. The state system is then determined:

$$A = \begin{bmatrix} -1.667 & 2.8339 & 0 \\ 0.0589 & -0.1001 & -0.0589 \\ 0 & 0 & -1.667 \end{bmatrix}, \quad B = \begin{bmatrix} 0.00672 \\ 0 \\ 0.005 \end{bmatrix}, \quad \Delta f = \begin{bmatrix} 0.2 \\ 0.2 \\ 1 \end{bmatrix} \zeta, \quad (10)$$

where it is assumed that  $\zeta$  is a bounded random signal that satisfies  $|\zeta| < 0.01$ .

Figure 5 illustrates  $V_t$  and  $I$  curves using the parameters provided by kim *et al.* [7], the cell modeling was done on Matlab/Simulink. For this particular test, the discharge current (5 A) was applied for 360 s (this discharges approximately 0.5 Ah from the battery since  $5 \text{ A} \times 360 \text{ s} = 0.5 \text{ Ah}$ ) and resting for 600 s to allow the terminal voltage relaxation towards the OCV. Each pulse current discharges approximately 10% of the nominal capacity, which is equivalent to 10% of the SOC reduction (since  $0.5 \text{ Ah} / 5 \text{ Ah} = 10\%$ ). The pulse current discharge and recovery was repeated until the terminal voltage reached the cut-off voltage of 2.5 V as the battery fully discharged (SOC = 0%).

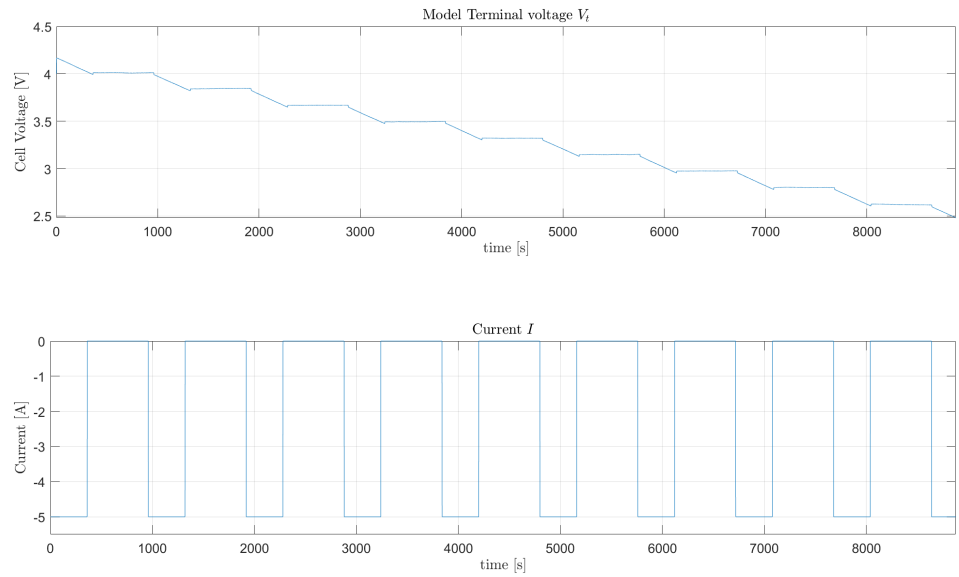


**Figure 5.** Terminal voltage and current curves for the cell model

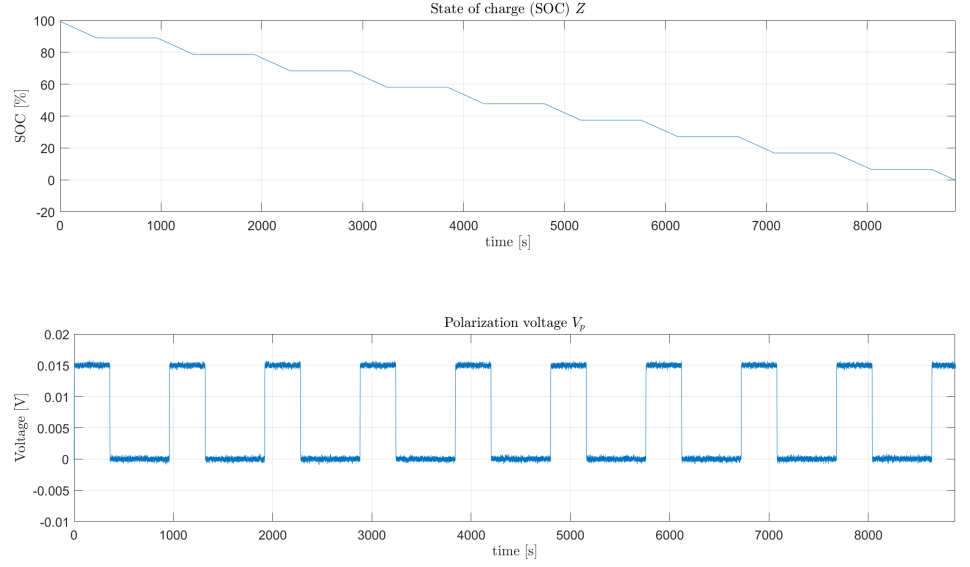


**Figure 6.** State of charge and Polarization voltage plot for the cell model

The voltage relaxation during rest periods tells us the polarization effects and diffusion processes within the battery. Each terminal voltage during relaxation time can be modelled as [9]:

$$V_t(t) = V_{oc} + V_p \exp\left(-\frac{t}{\tau_p}\right) \quad (11)$$

where  $\tau_p$  is the time constants for the polarization voltages  $V_p$  during transient response.  $V_{oc}$  is the OCV after complete relaxation. According to the battery model circuit analysis, the following equations are derived to calculate the parameters:

$$R_p = \frac{V_p}{I} \quad (12)$$

$$C_p = \frac{\tau_p}{R_p} \quad (13)$$

The terminal resistance is given by

$$R_t = \frac{\Delta V_t}{I} \quad (14)$$

where  $\Delta V_t$  is the difference between the terminal voltage and the OCV, and  $I$  is the discharge current.

#### 4. Observers Implementation

As the battery model can be considered an invariant linear system, three types of observers were implemented to compare the convergence and accuracy of different estimation techniques based on observation. Since each observer needs a gain matrix, the LQ method is developed to obtain the optimal gain values. The Riccati equation is applied as in [7]

$$AP + PA^T - PC^T R^{-1} CP = -Q \quad (15)$$

Where the positive definite solutions  $P$  leads to the computation of the gain matrix  $H$ :

$$H^T = R^{-1} CP \quad (16)$$

Choosing the values of  $R = 1$  and  $Q = I_3$  (3 by 3 identity matrix), then the positive definite solution of Riccati equation is:



$$P = \begin{bmatrix} 1.3629 & 0.9530 & -0.0046 \\ 0.9530 & 1.02441 & -0.0077 \\ -0.0046 & -0.0077 & 0.2999 \end{bmatrix} \quad (17)$$

Replacing the value of  $P$  on Equation (16):

$$H = \begin{bmatrix} h_1 \\ h_2 \\ h_3 \end{bmatrix} = \begin{bmatrix} 1.3629 \\ 0.9530 \\ -0.0046 \end{bmatrix} \quad (18)$$

#### 4.1 Luenberger Observer (State Observer) Design

The Luenberger observer is among one of the most implemented state algorithms, it is based on model and the feedback tracking error [12]. The so-called Luenberger observer was firstly proposed to tackle state estimation for linear deterministic dynamic systems [13]. The main idea of this observer is to generate a copy of the original system, in this case the battery model, from which one can measure the internal state, in this case  $V_t$ , and applying a correction factor multiplied by the constant values inside the gain matrix  $H$ . Thus, the difference between the system and the observer will tend to zero when time tends to infinity.

With the state space representation of the battery model presented in Equation (6), the corresponding LO is expressed as:

$$\dot{\hat{x}} = A\hat{x} + Bu + H(y - \hat{y}), \quad (19)$$

where  $y - \hat{y}$  represents the estimation error  $e_1$ , which depends on the difference between the real value of the terminal voltage and its estimation, which is:

$$e_1 = V_t - \hat{V}_t. \quad (20)$$

Using the state-space representation of the lithium-ion battery model in equation 6. The Luenberger Observer introduces a correction term to the dynamics as in equation 19. Expanding the observer equations we have:

$$\begin{aligned} \dot{\hat{V}}_t &= -a_1 \hat{V}_t + a_1 k \hat{Z} + b_1 I + h_1 (V_t - \hat{V}_t), \\ \dot{\hat{Z}} &= a_2 \hat{V}_t - a_2 k \hat{Z} - a_2 \hat{V}_p + h_2 (V_t - \hat{V}_t), \\ \dot{\hat{V}}_p &= -a_1 \hat{V}_p + b_2 I + h_3 (V_t - \hat{V}_t). \end{aligned} \quad (21)$$

The final estimated state equations for the battery model :

$$\begin{aligned} \dot{\hat{V}}_t &= -a_1 \hat{V}_t + a_1 k \hat{Z} + b_1 I + h_1 e_1, \\ \dot{\hat{Z}} &= a_2 \hat{V}_t - a_2 k \hat{Z} - a_2 \hat{V}_p + h_2 e_1, \\ \dot{\hat{V}}_p &= -a_1 \hat{V}_p + b_2 I + h_3 e_1, \end{aligned} \quad (22)$$

#### 4.2 Sliding Mode Observer Design

The SMO presents robust tracking performance under modeling uncertainties and disturbances such as noises, with a simple control structure [7]. Sliding mode is characterised by the implementations of a decision rule, called switching function. A feedback switching gain is designed to control sliding regime to guarantee robustness. Lyapunov stability theory is applied for verifying the error convergence [6]



A sliding mode observer for the system Eq. 6 is

$$\dot{\hat{x}} = A\hat{x} + Bu + H \text{sign}(y - \hat{y}) \quad (23)$$

where the gain matrix  $H$  and the switching gain  $\rho$  are chosen so that the stability of the observer system is preserved. The discontinuous feedback input is defined as

$$\text{sign}(e) = \begin{cases} +1, & e > 0 \\ -1, & e < 0 \end{cases} \quad (24)$$

The state error is defined as  $e = x - \hat{x}$ .

$$e_y = y - \hat{y} = Ce \quad (25)$$

The feedforward gain matrix  $H$  can be obtained in two ways: pole assignment method and LQ method. The LQ method is easier to obtain gain matrix  $H$  using the Riccati equation as in eq. 15

The estimated state equations for the battery model using the sliding mode observer algorithm is:

$$\begin{aligned} \dot{\hat{V}}_t &= -a_1 \hat{V}_t + a_1 K \hat{Z} + b_1 I + h_1 \text{sign}(\text{err}), \\ \dot{\hat{Z}} &= a_2 \hat{V}_t - a_2 K \hat{Z} - a_2 \hat{V}_p + h_2 \text{sign}(\text{err}), \\ \dot{\hat{V}}_p &= -a_1 \hat{V}_p + b_2 I + h_3 \text{sign}(\text{err}). \end{aligned} \quad (26)$$

### 4.3 Super Twisting Observer Design

Sliding mode control provides several techniques for designing controllers that are robust concerning a wide range of un-modeled disturbances. The ST algorithm is a very popular control algorithm in this regard [14]. To avoid the chattering effect on conventional SMO, several methodologies are proposed in sliding mode literature, ST algorithm is one of them. Other advantages of this method are: applies to systems where control appears in the first derivative of the sliding variable, compensates uncertainties and perturbations, require only information of the output, provides finite-time convergence, generates continuous control signal and, consequently adjusts the chattering [15].

$$\begin{aligned} \dot{\hat{V}}_t &= -a_1 \hat{V}_t + a_1 k \hat{Z} + b_1 I + h_1 |e_1|^{2/3} \text{sign}(e_1), \\ \dot{\hat{Z}} &= a_2 \hat{V}_t - a_2 k \hat{Z} - a_2 \hat{V}_p + h_2 |e_1|^{1/3} \text{sign}(e_1), \\ \dot{\hat{V}}_p &= -a_1 \hat{V}_p + b_2 I + h_3 \text{sign}(e_1). \end{aligned} \quad (27)$$

As shown in Equation (27), the correction terms were applied taking the values inside the matrix  $H$  as the observer gains.

## 5. Simulatuion Results for Terminal Volatge, SOC and Polarization Volatge Estimations

### 5.1 Constant Current Discharge Profile

For this paper, this discharge sequence is selected to perform faster computations. The discharge current of 5 A is applied every 960 s for a period of 360 s, leaving 600 s for rest. The results obtained from the implementations of the three observers are on Figures 7, 8 and 9 where each estimation is behaving like the model does.

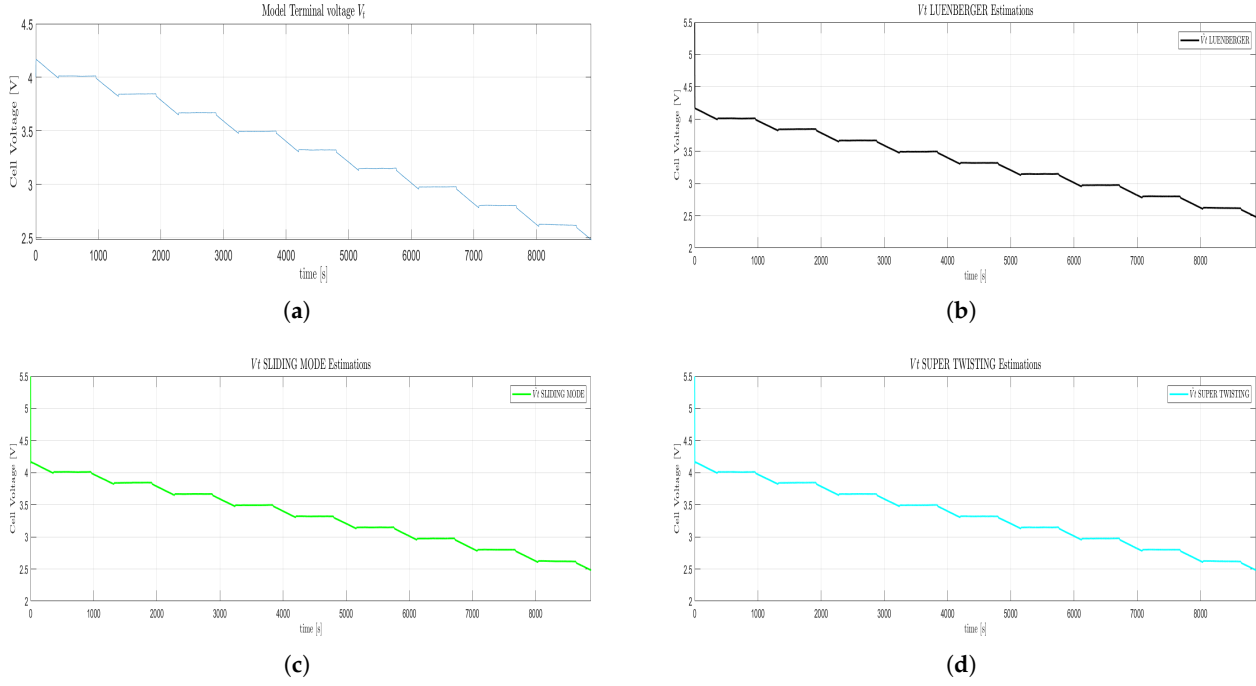


**Figure 7.** Model and estimations of terminal voltage  $V_t$ : (a) Model Terminal Voltage. (b) Luenberger Terminal Voltage Estimation. (c) Sliding Mode Terminal Voltage Estimation. (d) Super Twisting Terminal Voltage Estimation.

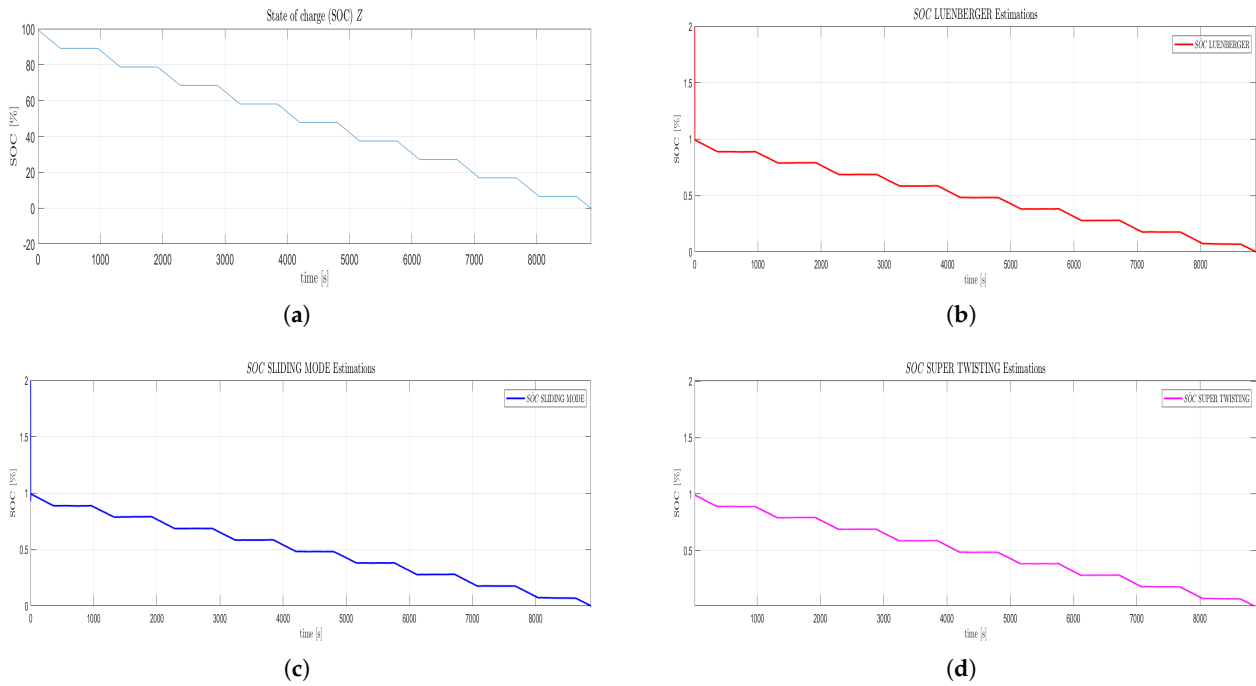


**Figure 8.** Model and estimations of State of Charge: (a) Model SOC. (b) Luenberger SOC Estimation. (c) Sliding Mode SOC Estimation. (d) Super Twisting SOC Estimation.

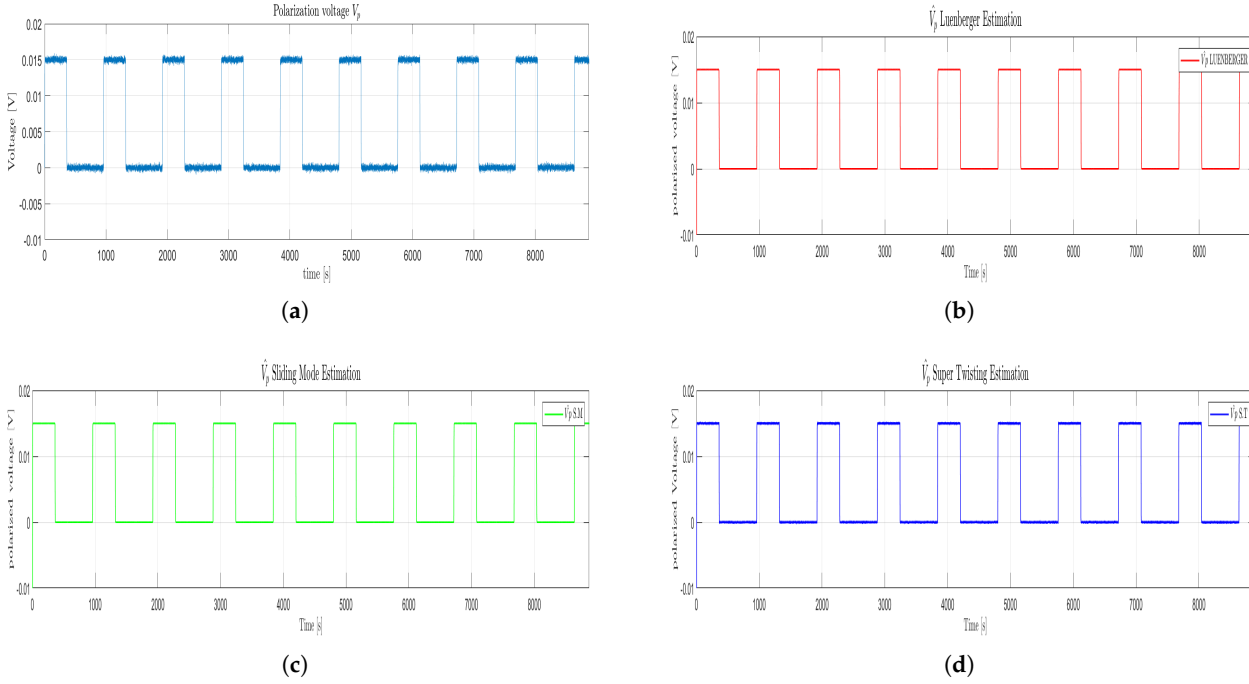


**Figure 9.** Model and estimations of Polarization Voltage  $V_p$ : (a) Model  $V_p$ . (b) Luenberger  $V_p$  Estimation. (c) Sliding Mode  $v_p$  Estimation. (d) Super Twisting  $V_p$  Estimation.

A complementary comparison table is developed with the computation of two control measures: Integral Squared Error (ISE) and Integral Absolute Error (IAE). Both measures are described in Equations (28) and (29). As mentioned, the ISE uses the integral of the squared error, which means that small fractions of error will not impact the final result in the measure. The opposite occurs in the IAE measure, as each absolute error contributes to the final result.

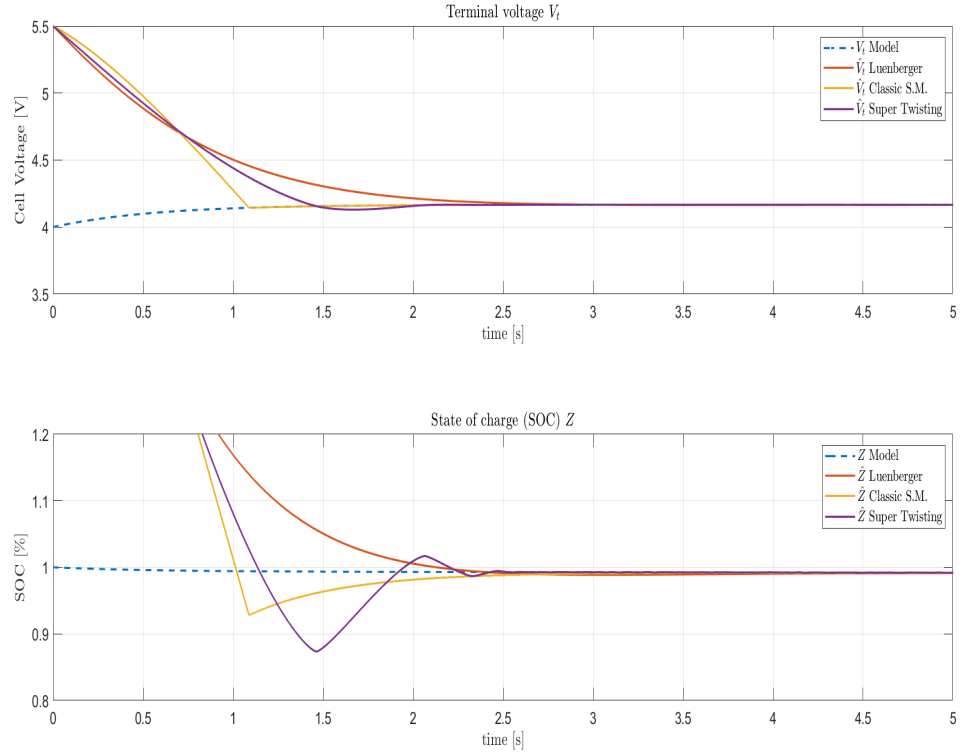
$$ISE = \int e^2 dt. \quad (28)$$

$$IAE = \int |e| dt. \quad (29)$$

**Table 1.** Estimation errors comparison for the constant current profile

	Luenberger		SMO		STO	
	ISE	IAE	ISE	IAE	ISE	IAE
$V_t$	0.8438	1.4136	0.8957	2.9851	0.8577	0.9673
$Z$	0.3052	0.8679	0.3356	2.0064	0.3258	1.8184
$V_p$	0.3017	2.0284	0.3017	2.0276	0.3018	2.1951

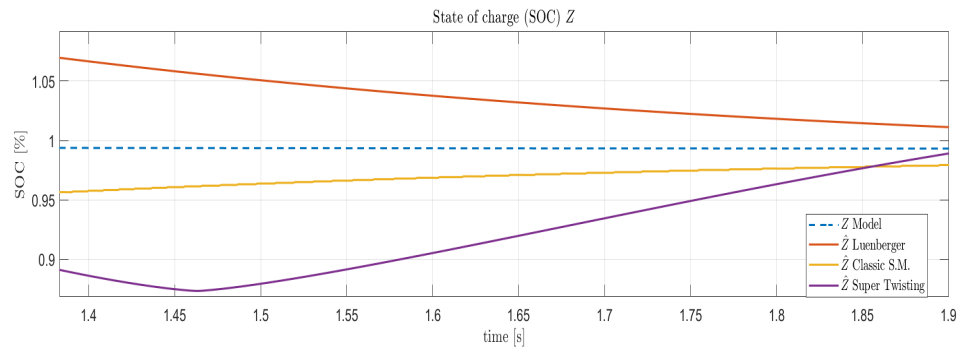
Figure 10 shows the behavior of the three observers during the first seconds of the simulation. The initial conditions of each observer are higher than the initial value of the model state to get a better appreciation of convergence. While the SMO and STO achieve the state between 1 s and 2 s, the Luenberger observer has an exponential-like curve which intersects the state at  $t \approx 2.5$  s.



**Figure 10.** Luenberger, SMO, and STO convergence curves.

Figure 11 presents a close look at the convergence curves of the SOC estimation. In the classic SMO, the curve has a small chattering as expected (simulation sampled time 1 ms), and furthermore, the super twisting observer complies with the proposal to reduce the chattering caused by the  $\text{sign}(y - \hat{y})$  function.

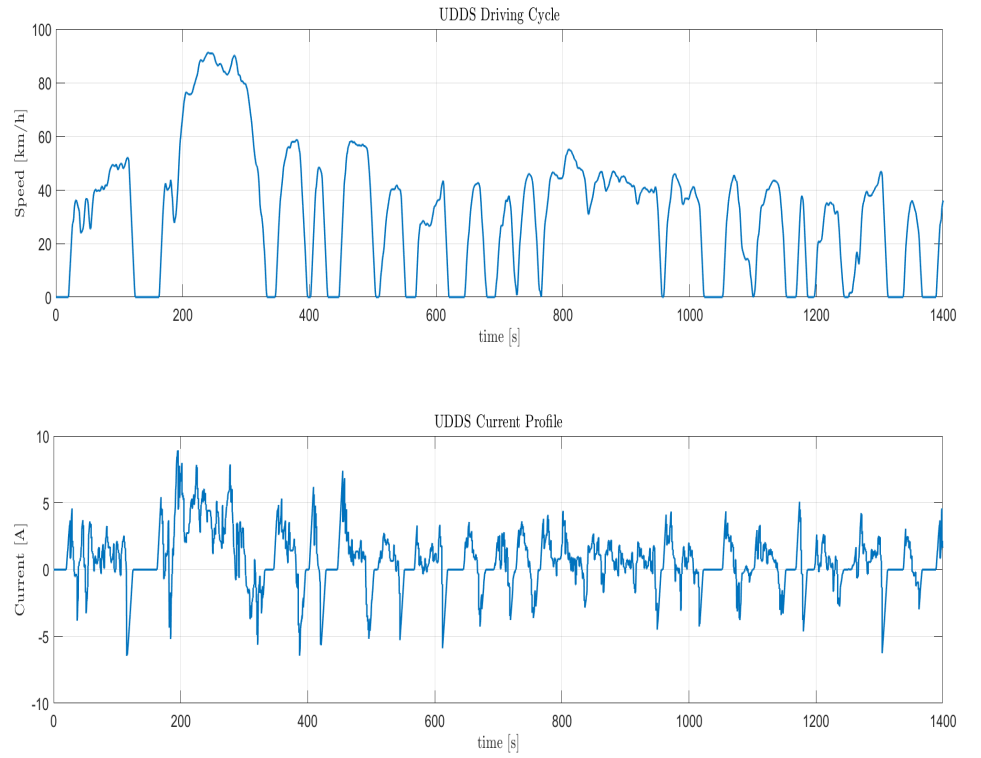
Table 1 presents the computation of the ISE and IAE errors for each observer. Overall, the results are satisfactory in the way that all observers converge to the target in finite time, and all three have similar accuracy tracking the model curves  $V_t$ ,  $Z$ , and  $V_p$ .



**Figure 11.** SMO chattering in SOC estimation.

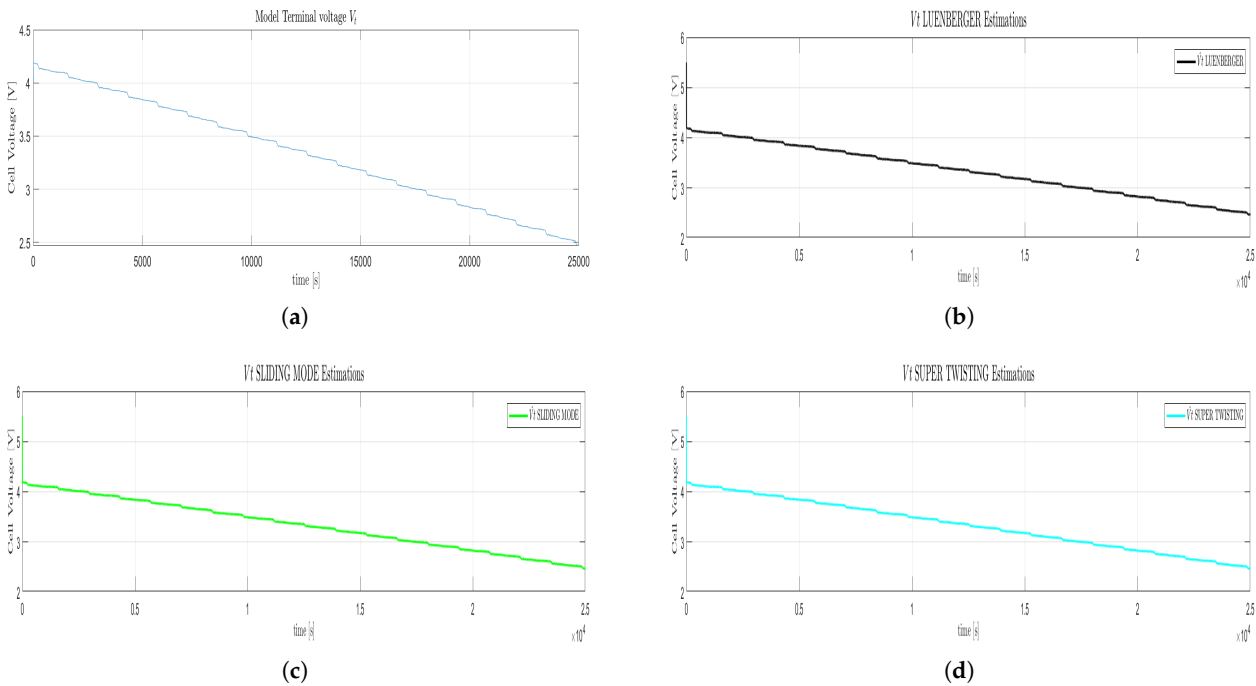
## 5.2 UDDS Current Profile

The Urban Dynamometer Driving Schedule (UDDS) cycle is used to simulate a more realistic discharge/charge current profile. The cycle reproduces an urban route of 12.07 kilometers distance with frequent stops, reaching a maximum speed of 91.25km/h and an average speed of 31.5km/h. Figure 12 presents one UDDS cycle speed and current profile, which has a total period of 1372 seconds. The negative current during the deceleration and braking of the EVs represents regenerative energy to charge the battery [16].

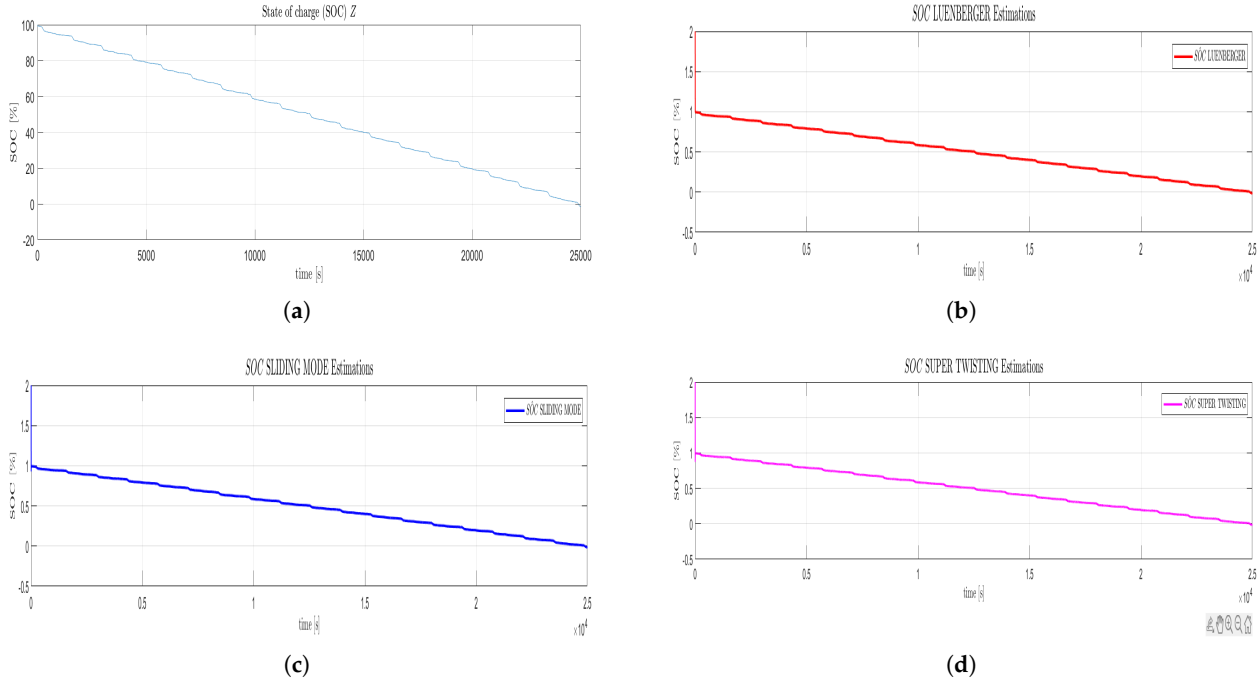


**Figure 12.** One UDDS cycle with corresponding current profile.

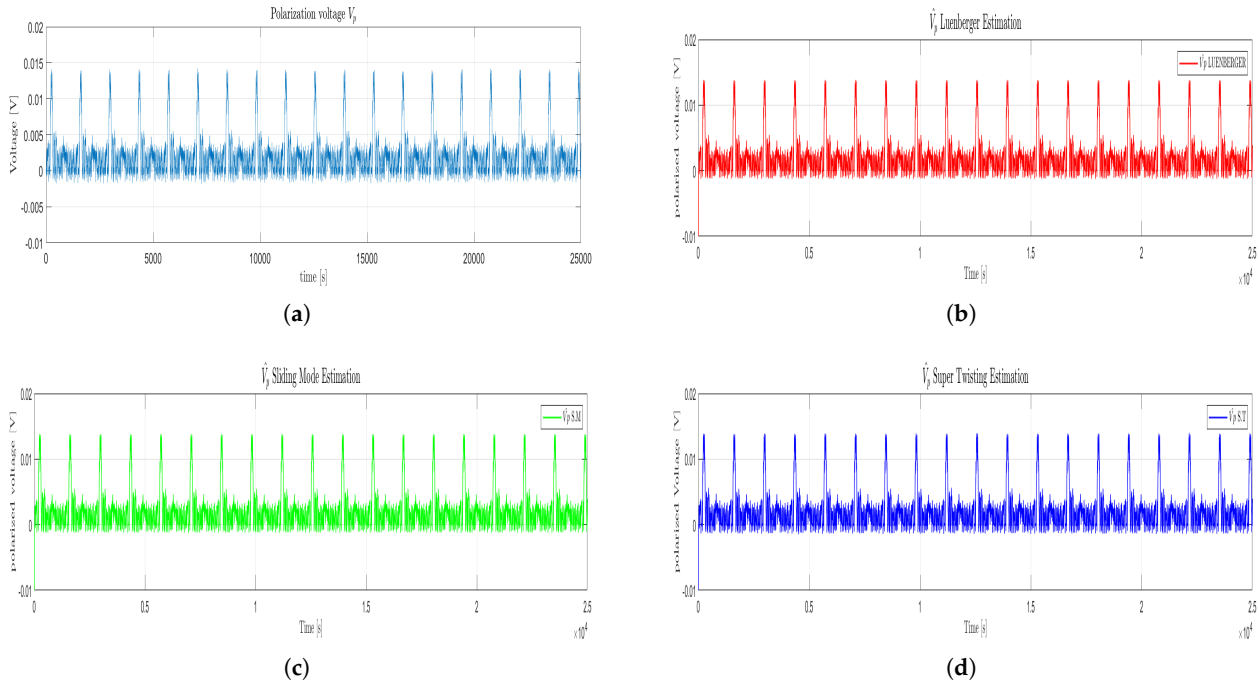
The UDDS current profile is applied to the battery until it reaches its cut-off voltage around 2.5 V, and each UDDS cycle discharges approximately 5% of the battery charge. Figures 13, 14, and 15 show the curves  $V_t$ ,  $Z$ , and  $V_p$  from the cell model and the estimation of each observer. Hence, the three observers are able to track the model's output even when a more accurate current profile is applied.



**Figure 13.** Model and estimations of terminal voltage  $V_t$  under UDDS profile: (a) Model Terminal Voltage. (b) Luenberger Terminal Voltage Estimation. (c) Sliding Mode Terminal Voltage Estimation. (d) Super Twisting Terminal Voltage Estimation.



**Figure 14.** Model and estimations of State of Charge under UDDS profile: (a) Model SOC. (b) Luenberger SOC Estimation. (c) Sliding Mode SOC Estimation. (d) Super Twisting SOC Estimation.

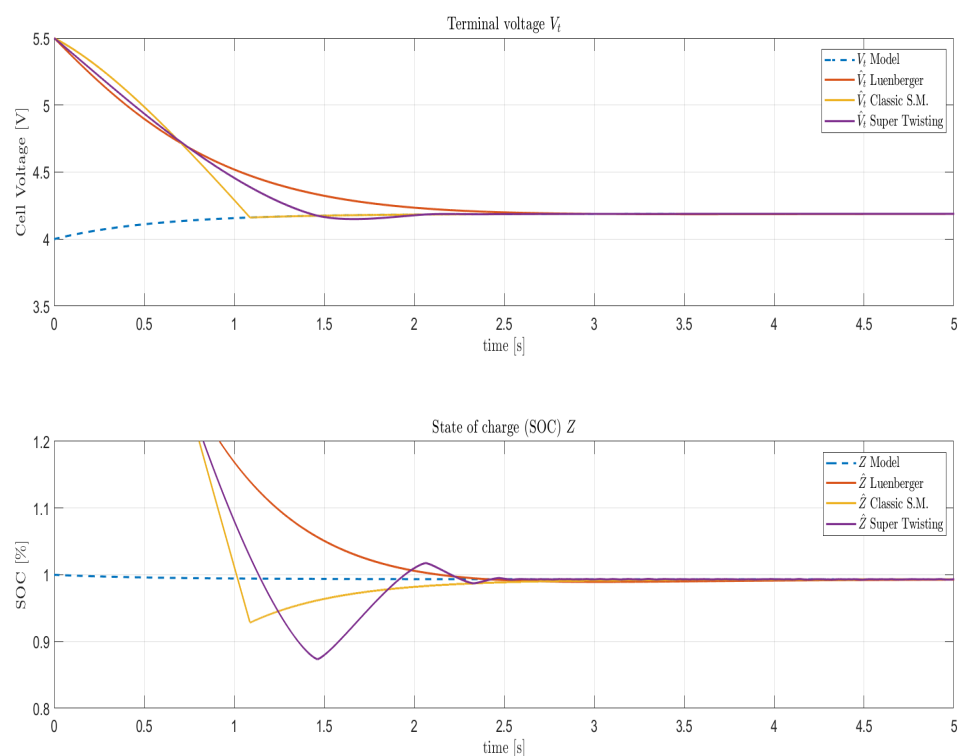


**Figure 15.** Model and estimations of Polarization Voltage  $V_p$  under UDDS profile: (a) Model  $V_p$ . (b) Luenberger  $V_p$  Estimation. (c) Sliding Mode  $v_p$  Estimation. (d) Super Twisting  $V_p$  Estimation.

**Table 2.** Estimation errors comparison for UDDS current profile

	Luenberger		SMO		STO	
	ISE	IAE	ISE	IAE	ISE	IAE
$V_t$	0.8438	2.1084	0.8971	6.8321	0.8577	1.0472
$Z$	0.3053	1.4025	0.3362	4.6641	0.3263	4.0959
$V_p$	0.3023	4.5814	0.3023	4.5792	0.3026	5.0604

Figure 16 shows the convergence for the Luenberger observer, SMO, and STO for the UDDS current profile. Furthermore, Table 2 presents the convergence errors, and it is observed that the SMO presents the highest IAE errors. For the IAE measure, the small fractions of errors were taken into consideration, and they have an impact on the final result as previously mentioned, which does not happen for the ISE measure. Moreover, this behavior is due to the simulation sampled time of  $1e-3$  and the new current profile providing more realistic and fast changes in the current. The sampled time could not be higher due to computational limitations.

**Figure 16.** Luenberger, SMO, and STO convergence curves under UDDS profile.

## 6. Conclusion

The importance of an accurate SOC estimation for EV batteries has been highlighted. Among all the existent methodologies, the robustness against modeling errors and uncertainties makes the SMO method a reliable and wide accepted technique for on-line applications. For battery modeling the EECM approach of RC model, even though it is not completely accurate, gives a valuable simulation of a real battery discharge behavior.

When applying different observers, all the same gain matrix, each of them performs a good estimation of the model. During the first seconds one can appreciate that the convergence of SMO observer is the fastest one, followed by STO. The error measurements tables have very similar values for the three observers. One can even think that the Luenberger observer is better than the others considering the ISE and IAE errors. However, for real applications this observer is not recommended due to the non-linearities and uncertainties of a real battery. Thus, while the SMO shows an evident high-speed convergence and



Luenberger observer has an exponential behavior, when talking about on-line applications the SMO and STO are better options thanks to the their high frequency action.

For the approach presented in this paper the gain values of SMO and STO can be changed for higher values to perform a closer state estimation. However, model state estimations is not the final goal, and to give a SOC estimation of a real battery with the lowest error possible one must do tests to a real system.

**Author Contributions:** Conceptualization, Qudus Ayinde Aromose and Stefan George Rosu; Methodology, Qudus Ayinde Aromose; Software, Qudus Ayinde Aromose; Validation, Qudus Ayinde Aromose and Stefan George Rosu; Formal Analysis, Qudus Ayinde Aromose; Investigation, Qudus Ayinde Aromose; Resources, Stefan George Rosu; Data Curation, Qudus Ayinde Aromose; Writing—Original Draft Preparation, Qudus Ayinde Aromose; Writing—Review and Editing, Qudus Ayinde Aromose and Stefan George Rosu; Visualization, Qudus Ayinde Aromose; Supervision, Stefan George Rosu; Project Administration, Stefan George Rosu.

All authors have read and agreed to the published version of the manuscript..

**Funding:** “This research received no external funding”

**Conflicts of Interest:** “The authors declare no conflicts of interest.”

## References

1. United Nations Framework Convention on Climate Change (UNFCCC). The Paris Agreement. <https://unfccc.int/process-and-meetings/the-paris-agreement>, 2024. Accessed: 2024-12-19.
2. UK Government. COP26 Declaration on Accelerating the Transition to 100 [https://www.gov.uk/government/publications/cop26-declaration-zero-emission-cars-and-vans/](https://www.gov.uk/government/publications/cop26-declaration-zero-emission-cars-and-vans/cop26-declaration-on-accelerating-the-transition-to-100-zero-emission-cars-and-vans), 2024. Accessed: 2024-12-19.
3. Shrivastava, P.; Soon, T.K.; Idris, M.Y.I.B.; Mekhilef, S. Overview of model-based online state-of-charge estimation using Kalman filter family for lithium-ion batteries. *Renewable and Sustainable Energy Reviews* **2019**, *113*, 109233.
4. Liu, K.; Li, K.; Peng, Q.; Zhang, C. A brief review on key technologies in the battery management system of electric vehicles. *Frontiers of mechanical engineering* **2019**, *14*, 47–64.
5. Yilmaz, M.; Krein, P.T. Review of battery charger topologies, charging power levels, and infrastructure for plug-in electric and hybrid vehicles. *IEEE transactions on Power Electronics* **2012**, *28*, 2151–2169.
6. Hannan, M.A.; Lipu, M.H.; Hussain, A.; Mohamed, A. A review of lithium-ion battery state of charge estimation and management system in electric vehicle applications: Challenges and recommendations. *Renewable and Sustainable Energy Reviews* **2017**, *78*, 834–854.
7. Kim, I.S. The novel state of charge estimation method for lithium battery using sliding mode observer. *Journal of Power Sources* **2006**, *163*, 584–590.
8. Hannan, M.A.; Hoque, M.M.; Hussain, A.; Yusof, Y.; Ker, P.J. State-of-the-art and energy management system of lithium-ion batteries in electric vehicle applications: Issues and recommendations. *Ieee Access* **2018**, *6*, 19362–19378.
9. Chen, X.; Shen, W.; Cao, Z.; Kapoor, A. A novel approach for state of charge estimation based on adaptive switching gain sliding mode observer in electric vehicles. *Journal of Power Sources* **2014**, *246*, 667–678.
10. Xiong, R.; Cao, J.; Yu, Q.; He, H.; Sun, F. Critical review on the battery state of charge estimation methods for electric vehicles. *Ieee Access* **2017**, *6*, 1832–1843.
11. Ogata, K. *Modern Control Engineering*; Instrumentation and controls series, Prentice Hall, 2010.
12. He, T.; Li, D.; Wu, Z.; Xue, Y.; Yang, Y. A modified luenberger observer for SOC estimation of lithium-ion battery. In Proceedings of the 2017 36th Chinese control conference (CCC). IEEE, 2017, pp. 924–928.
13. Hu, X.; Sun, F.; Zou, Y. Estimation of state of charge of a lithium-ion battery pack for electric vehicles using an adaptive Luenberger observer. *Energies* **2010**, *3*, 1586–1603.

14. Seeber, R.; Horn, M. Stability proof for a well-established super-twisting parameter setting. *Automatica* **2017**, *84*, 241–243. 320
15. Chalanga, A.; Kamal, S.; Fridman, L.M.; Bandyopadhyay, B.; Moreno, J.A. Implementation of super-twisting control: Super-twisting and higher order sliding-mode observer-based approaches. *IEEE Transactions on Industrial Electronics* **2016**, *63*, 3677–3685. 321
16. Chen, X.; Shen, W.; Cao, Z.; Kapoor, A. Adaptive gain sliding mode observer for state of charge estimation based on combined battery equivalent circuit model. *Computers & Chemical Engineering* **2014**, *64*, 114–123. 322